Nonlinear Model Updating for Riveted Joints

Josh Blackham[1], Cameron Stoker[2], Matthew S. Allen[3], and Brandon Rapp[4]

[1]Graduate Student, Brigham Young University, Department of Mechanical Engineering, jeb419@byu.edu
[2]Undergraduate Student, Brigham Young University, Department of Mechanical Engineering, stoke29@byu.edu
[3]Professor, Brigham Young University, Department of Mechanical Engineering, matt.allen@byu.edu
[4]Structures Engineer, Pratt & Whitney, brandon.rapp@prattwhitney.com

Abstract

Nonlinear modeling of joints is often difficult to do accurately because of various small-scale and nonlinear features, such as local geometry, surface shape, preload and friction. These features cause a local change in stiffness and energy dissipation which result in changes in the effective natural frequency and damping of the whole structure. Past studies have found good success using nonlinear Iwan elements as whole joint models for bolted joints in a few different structures. In this paper, a similar approach is proposed for modeling riveted joints, which seeks to capture the vibrational response of a test structure including changes in the effective modal frequency and damping with vibration amplitude. A four parameter, nonlinear Iwan element is used to model each rivet joint in the test structure. The rest of the structure is modeled using a linear finite element model (FEM), which is reduced using interface spiders and the Hurty/Craig-Bampton method to speed up simulations. The Quasi-Static Modal Analysis (QSMA) approach is used to find the effective mode frequencies, shapes, and damping as a function of vibration amplitude. These results are then compared to experimental measurements of the impact excited response on a test structure to validate the model accuracy.

Keywords: Nonlinear, Iwan Element, Rivet

1 Introduction

Joints in structures serve a practical purpose by allowing large, complex structures to be built from smaller, simpler pieces and making it possible to disassemble components for maintenance or to replace a part. Joints also add friction and damping to the structure [1], reducing the vibration amplitudes and potentially avoiding catastrophic failure. Quite a bit of research has been performed seeking to understand how these interfaces [2, 3], and in particular, bolted joints in structures, influence the effective damping and natural frequencies of vibration modes in assembled structures. Many recent works have found that the nonlinearity that they introduce causes these effective properties to change with vibration amplitude or with the level of excitation applied [4, 5].

One particular model that has been used and developed to predict amplitude-dependent changes in effective damping and natural frequency is the 4 parameter Iwan element. Originally developed by Iwan [6], the element has as a series of friction sliders (Jenkins elements) that capture the hysteresis in a joint by allowing a certain fraction of the elements to slip under a given load while the rest remain stuck and cause the joint to have a certain stiffness. Segalman [7] later expanded on this, creating a 4 parameter Iwan element that has been used often in recent work.

The 4 parameter Iwan element has been successful at modeling joints in structures, but the identification of the 4 parameters in the model tends to be quite difficult. Festjens et al. [8] proposed a quasi-static modal analysis (QSMA) method that involves forcing the structure in the shape of a particular mode and then using the nonlinear static response to infer the dynamic behavior at various forcing amplitudes. Specifically, Masing's rules are used to infer the response over one loading and unloading cycle from the quasi-static force-displacement behavior. This can then be related to the dynamic response as the structure vibrates in the particular mode of interest. This allows one to compute the amplitude dependent natural frequency and damping while avoiding the computational expense required to integrate the equations of motion to find the dynamic response. Lacayo and Allen [9] simplified their approach and showed that it could be applied to a reduced model with Iwan elements in place of the bolted joints. QSMA then allowed the effective natural frequency and damping to be computed very efficiently. They measured the amplitude dependent frequency and damping of a mode of the structure of interest and then used an optimization approach to iteratively find the 4 parameters in the Iwan elements that best reproduced the measured response.

Singh et al. [10] introduced a simple benchmark structure called the S4 beam that was tested at various amplitudes of excitation and yielded significant nonlinearities in natural frequency and damping of different modes of the structure. Later, using Lacayo's

method of QSMA, Singh et al. [11] modeled the S4 beam and matched the model's amplitude-dependent frequency and damping to the previously measured experimental data in [10]. Specifically, Singh et al. [11] began with a full-order finite element model of the S4 beam. They then applied the Hurty/Craig-Bampton method to reduce the full-order model and created multi-point constraints to simplify the joint interfaces. Linear springs were inserted into the reduced model at the joint locations to match the low amplitude experimental mode frequencies. A Monte Carlo optimization then found Iwan parameters for the 4 parameter Iwan joint used in QSMA, using the optimized stiffness of the linear springs as the value for the Iwan parameter, K_t. In [11], the focus of the work was how different multi-point constraints in the FEM affect the model and the Iwan element stiffness parameter, K_t. One important finding was that some multi-point constraints yielded higher linear spring stiffnesses during the linear optimization. These high spring stiffnesses made it impossible to find a set of Iwan parameters that were capable of matching the model to the experiments during the nonlinear optimization and QSMA.

This paper builds on that in [11], focusing on how Iwan elements perform when modeling rivets instead of bolts, since rivets join two structures in a distinct manner. Whereas bolts apply a normal pressure to the plate during pretension, rivets apply a radial pressure to the rivet hole [12]. Using the previously developed QSMA methods, an Iwan element will be used to model each rivet in a simple test structure, and then optimization will be used to match the nonlinear frequency and damping behavior of the first mode to experimental measurements.

2 Theory

This section discusses the process that was used in this study to find a nonlinear model for the riveted joints. A finite element model (FEM) was first built in the Abaqus commercial finite element analysis (FEA) package. The FEM was reduced using the Hurty/Craig Bampton (HCB) method and the resulting mass and stiffness matrices were exported to Matlab for further analysis. Using Matlab's *fminsearch* function, a set of best-fit linear springs were inserted in every degree of freedom at each joint by modifying the reduced stiffness matrix. The linear spring stiffnesses were then used as one of four Iwan parameters in a nonlinear model for the joints. The rest of the parameters were found using the quasi-static optimization approach used by Lacayo [13] and Singh [11], which uses a Monte Carlo approach to iterate on the rest of the parameters in the Iwan model until the best agreement is obtained between the measured natural frequency and damping versus amplitude and that predicted by the model.

2.1 Hurty/Craig Bampton Reduction

The Hurty/Craig Bampton (HCB) method reduces a large, complicated model to a smaller model that is quicker and more efficient to work with. A discussion of the general principles of HCB reduction [14, 15] will follow: Consider a full model whose undamped equation of motion is given by Equation 1, where $\mathbf{M}$ is the full order mass matrix, $\mathbf{K}$ is the full order stiffness matrix, $\mathbf{F}$ is a vector of applied forces, $\mathbf{F}_J(\mathbf{u}, \theta)$ is the source of nonlinearity in the system, and $\mathbf{u}$ and $\ddot{\mathbf{u}}$ are the physical displacement and acceleration, respectively.

$$\mathbf{M}\ddot{\mathbf{u}} + \mathbf{K}\mathbf{u} + \mathbf{F_J}(\mathbf{u}, \theta) = \mathbf{F} \tag{1}$$

The mass and stiffness matrices are partitioned into boundary and internal degrees of freedom (DOFs) as follows:

$$\begin{bmatrix} \mathbf{M}_{ii} & \mathbf{M}_{ib} \\ \mathbf{M}_{bi} & \mathbf{M}_{bb} \end{bmatrix} \begin{Bmatrix} \ddot{\mathbf{u}}_i \\ \ddot{\mathbf{u}}_b \end{Bmatrix} + \begin{bmatrix} \mathbf{K}_{ii} & \mathbf{K}_{ib} \\ \mathbf{K}_{bi} & \mathbf{K}_{bb} \end{bmatrix} \begin{Bmatrix} \mathbf{u}_i \\ \mathbf{u}_b \end{Bmatrix} + \begin{Bmatrix} 0 \\ \mathbf{F}_{J,b}(\mathbf{u}_b) \end{Bmatrix} = \begin{Bmatrix} 0 \\ \mathbf{F}_b \end{Bmatrix} \tag{2}$$

where the subscript *i* denotes the internal DOF and *b* denotes a boundary DOF. It is assumed that the nonlinearity and any forces are applied only at the boundary locations; the nonlinear joints must also exert forces only between the boundary DOF. The interfaces of the structure are described by a set of static constraint modes, ψ, which are the responses of the structure with each interface DOF displaced one unit. The interior of the structure is defined by a set of fixed interface modes (FIM), ϕ, which are the vibrational modes with every interface DOF fixed. Thus a small number of FIMs and constraint modes can accurately and efficiently describe the structure. The combination of the FIMs and constraint modes can be used to form the HCB transformation matrix in Equation 3.

$$\begin{Bmatrix} \mathbf{u}_i \\ \mathbf{u}_b \end{Bmatrix} = \mathbf{T}^{\text{HCB}} \begin{Bmatrix} \mathbf{q}_i \\ \mathbf{u}_b \end{Bmatrix} = \begin{bmatrix} \boldsymbol{\Phi} & \boldsymbol{\Psi} \\ \mathbf{0} & \mathbf{I} \end{bmatrix} \begin{Bmatrix} \mathbf{q}_i \\ \mathbf{u}_b \end{Bmatrix} \tag{3}$$

In this work, the HCB reduction was performed using the *Substructure Generate* step in Abaqus FEA. The user must first specify the set of boundary nodes, which are retained. The set of boundary nodes was reduced further by using Multi-Point Constraints (MPCs) to connect all nodes within the joint to one reference (or virtual) node. See Figure 1 for an example of how these constraints connect a region of nodes to a reference node.

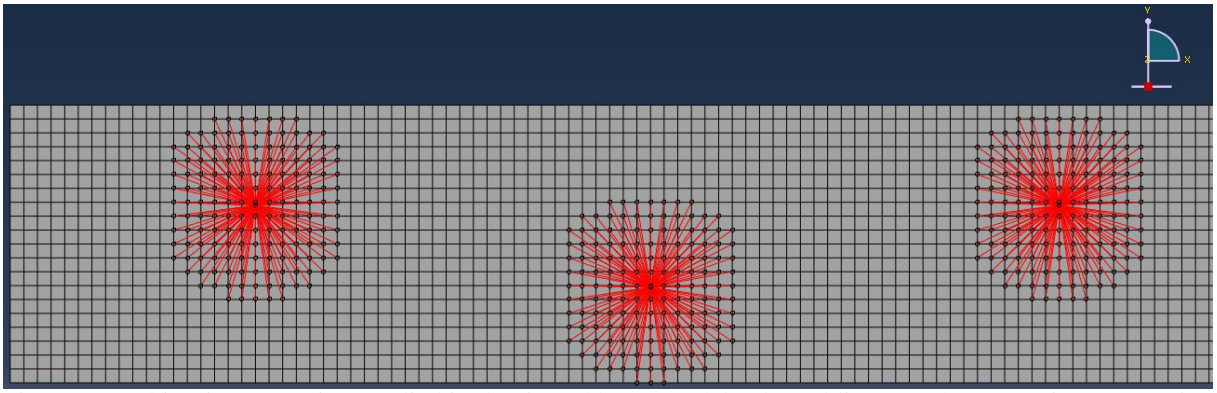

Figure 1: Multi-point constraints applied in the riveted beam model. The red lines are the constraints connecting each node within a defined radius to the reference node.

2.2 Linear Response Optimization

Once the FEM of the structure was built and the mass and stiffness matrices were reduced, the next step was to insert linear springs in place of the joints and then to adjust their stiffnesses to match the linear mode frequencies of the model to the experimental mode frequencies. This was done by adding the corresponding spring constant into the stiffness matrix at the indices of the degrees of freedom of the joint. Equation 4 shows how the spring stiffness can be added into the reduced stiffness matrices; this was implemented in a Matlab script.

$$\mathbf{K}(\mathbf{n},\mathbf{n}) = \mathbf{K}(\mathbf{n},\mathbf{n}) + K_s \begin{bmatrix} 1 & -1 \\ -1 & 1 \end{bmatrix} \tag{4}$$

where $\mathbf{K}$ is the reduced stiffness matrix, $\mathbf{n}$ is a length 2 vector representing the indices in the stiffness matrix of the two joints being connected, and K_s is the spring stiffness that is inserted between that pair of degrees of freedom. This was repeated for every pair of nodes that were joined by rivets, and in all six degrees of freedom. There are 24 rivets in the model, and each node representing a rivet location had 6 degrees of freedom, so there were a total of 6×24 springs inserted. The stiffnesses in the X and Y directions were assumed to be equal because the rivets are round and have the same geometry in both directions. The rotational stiffnesses in X and Y were also assumed to be equal, so there were a total of 4 unknown stiffness parameters. These were collected in a vector $\boldsymbol{\theta} = [K_x = K_y, K_z, R_x = R_y, R_z]^{\mathrm{T}}$.

Matlab's *fminsearch* function was used to optimize towards the minimum of the defined function, f($\boldsymbol{\theta}$), in Equation 5. This optimization finds the spring stiffnesses that minimize the root mean square error between experimental and model mode frequencies.

$$f(\boldsymbol{\theta}) = \sum_{i=1}^{n} \left(\frac{\omega_{\text{model},i}(\boldsymbol{\theta}) - \omega_{\text{exp},i}(\boldsymbol{\theta})}{\omega_{\text{exp},i}(\boldsymbol{\theta})} \right)^2 \tag{5}$$

where n is the number of vibration modes to match frequency.

The ultimate goal of the linear optimization is to find a model whose linear natural frequencies match with those measured experimentally at low vibration amplitudes. Once these optimized spring stiffnesses were found, the springs in the X and Y direction were replaced with Iwan elements and the value K_x was used as the K_t parameter, as elaborated in the next section.

2.3 Nonlinear Response Optimization

2.3.1 QSMA

Quasi-Static Modal Analysis (QSMA) was first developed by Festjens et al. [8] as an alternative to dynamic time integration of a FEM. In QSMA, a distributed force is applied at increasing amplitudes to excite a particular mode in question. The resulting force-displacement curve is then used to find the effective natural frequency and damping of the structure as it vibrates in the specific mode of interest over a range of vibration amplitude. In effect, the static response is used to infer the unforced response of the structure as the vibration decays in the mode in question. This process is much faster than a dynamic simulation of a FEM and is accurate as long as there is no modal coupling.

In [8], Festjens et al. split their model into a linear portion and a nonlinear portion and iterated on each until both solutions agreed at the interface. Lacayo and Allen [9] adjusted this QSMA approach by simply treating the whole model as the nonlinear

portion, thus avoiding the need to iterate. This potentially increases the computational cost, so Lacayo and Allen performed Hurty/Craig-Bampton reduction on the model and modeled the joints as four parameter Iwan elements [7]; In contrast, Fetjens et al. modeled the preload and contact in detail using Coulomb friction. Note that Jewel et al [16] later applied QSMA to a model in which the joints were modeled in detail, as done by Festjens et al.

The process used by Lacayo and Allen [9] is the same process used in this work and will be summarized here: We begin again with the equation of motion for the FEM of our structure with joints represented with a discrete, force constitutive model, $\mathbf{F_J}(\mathbf{u}, \boldsymbol{\theta})$.

$$\mathbf{M\ddot{u}} + \mathbf{Ku} + \mathbf{F_J}(\mathbf{u}, \boldsymbol{\theta}) = \mathbf{F} \tag{6}$$

The assumption is made that the structure is vibrating at the *r*th mode such that $\mathbf{u}(t) = \boldsymbol{\varphi_r}\sin(\omega_r t)$, where $\boldsymbol{\varphi_r}$ is the mode shape of the *r*th mode. The inertial term in Equation 6 is now proportional to $\mathbf{M}\boldsymbol{\varphi_r}$. The structure is allowed to vibrate freely such that $\mathbf{F} = 0$, and so the inertial term can be moved to the right hand side and treated as an applied distributed load that only excites one mode in the linear structure. This yields Equation 7.

$$\mathbf{Ku} + \mathbf{F_J}(\mathbf{u}, \boldsymbol{\theta}) = -\alpha\mathbf{M}\boldsymbol{\varphi_r} \tag{7}$$

which can be solved for the displacement $\mathbf{u}$ in terms of a monotonically increasing amplitude level, α.

After solving for the quasi-static response, $\mathbf{u}(\alpha)$, the amplitude-dependent modal frequency and damping ratio can be found using the same approach as Festjens et al. which comes from assumptions made using Masing's rules and the force-deflection hysteresis curve. In brief summary, the amplitude dependent stiffness is related to the natural frequency which comes from the slope of the secant line in the hysteresis plot, as given in Equation 8.

$$\omega_r(\alpha_j) \triangleq \sqrt{\frac{\alpha_j}{q_r(\alpha_j)}} \tag{8}$$

where $\omega_r(\alpha_j)$ is the natural frequency of the mode and $q_r(\alpha_j)$ is the modal displacement, which are both dependent on the amplitude of excitation, α_j. The amplitude dependent damping of the structure can be found using Equation 9.

$$\zeta_r(\alpha_j) \triangleq \frac{D(\alpha_j)}{2\pi\alpha_j q_r(\alpha_j)} \tag{9}$$

where $D(\alpha_j)$ is the total energy dissipated per cycle of vibration or the area enclosed by the Hysteresis curve after applying Masing's rules.

2.3.2 Monte Carlo Optimization

Optimization is used to find the four Iwan parameters that cause the natural frequency and damping versus amplitude of the reduced order model to best agree with measurements. The optimization has been found to be prone to getting stuck in local minima, so a Monte Carlo optimization strategy is used. Bounds are defined around each of the parameters, and then N_{MC} random samples are drawn from a uniform distribution defined by those bounds. QSMA is used to evaluate the weighted average error between the frequency and damping curves predicted by the model and the measured ones and the set of parameters that gives the best results is retained. The bounds are then contracted around the set of parameters that gave the best results and the optimization is repeated. The process ends when the optimization either reaches a prescribed accuracy or ceases to improve.

In the studies in this paper, we have typically used $N_{MC} = 100$ and after each set of iterations defined a new range for each parameter that is $\pm 3\%$ of the optimal value found in the previous step. The optimization described in Sec 2.2, ends by identifying an ideal tangential stiffness value, K_t. As a result, this parameter typically does not need to be varied over a large range. To simplify the process, K_T is varied by changing $\gamma \approx 1$ where $K_T = \gamma K_s$ and K_s is the value found in the first optimization for the spring that is being replaced by the Iwan element. The power-law slope χ has a clear effect on the damping curve so it typically only varies between $-1 < \chi < 1$. In contrast, the other two parameters F_S and β may need to be varied by several orders of magnitude to find the optimal value.

The approach above has worked well in some prior studies [11], yet it loses effectiveness if the parameter ranges are very large. When certain parameters are varied over a large range the response sometimes changes very little, but if the parameter is near the optimum it may be very sensitive to small changes. In the course of this work the authors have found it helpful to manually explore the search space using very wide parameter ranges before starting the optimization. This helps to ensure that the Monte Carlo algorithm will search in a space where the changes to the parameters can improve the response of the model.

3 Results

The test structure modeled for this study consisted of two long and slender beams joined together by 24 steel rivets set in an offset pattern along the length of the beams. All experimental data used in this work was collected as described in a companion paper by Gilbert et al. [17].

3.1 Riveted Beam Abaqus Model

Various iterations of the model were created in Abaqus to understand the effect of different modeling choices that can be made, such as whether to model the beams with shell or solid elements, what type of multi-point constraints to use, and other settings specific to the constraints and HCB substructuring procedure. A companion paper [18] explores the importance of the various modeling options. For this work, the beams were modeled using shell elements and the holes were ignored; this model is called the "Shell No Holes" model in [18]. The region near each rivet was constrained using *Distributing Uniform* type multi-point constraints. See Figure 1 for a picture of the model created in Abaqus.

3.2 Linear Spring Model

The approach described in Sec. 2.2 was used to find the stiffnesses of the linear springs that brought the model's natural frequencies into agreement with those from test. As the *fminsearch* function does this, it returns the value of the objective function ($f(\theta)$ in Eq. 5) and this can be monitored as the optimizer approaches best results. An example of this can be seen in Figure 2. Notice that around Iteration 40, the function value reaches a minimum and no longer improves significantly. It was found that even though the function value no longer improves, the spring stiffness continues to increase as the optimization continues to iterate. This can be seen in Table 1, which shows the stiffness K_x as the optimization advances.

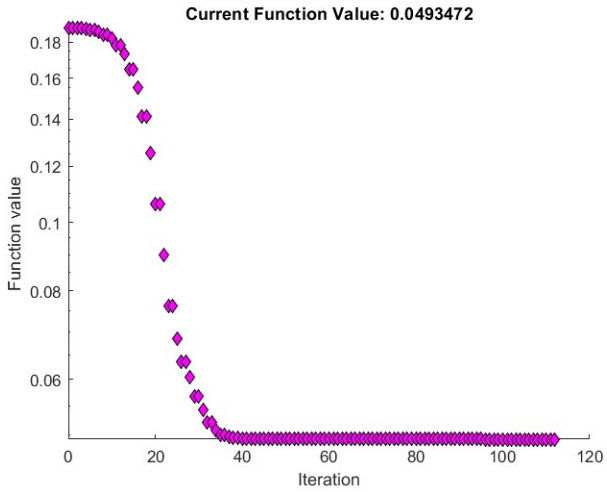

Figure 2: Plot of the *fminsearch* objective function value during linear optimization.

Table 1: Objective function value and normalized spring stiffness at various iterations of the linear optimization.

Iteration	$F(\theta)$	Stiffness K_x
30	0.056667	1
40	0.049434	168
50	0.049349	32372
60	0.049348	206730
70	0.049347	195510
80	0.049347	195510

Singh et al. [11] found that an Iwan element would contribute little damping to the assembly if its stiffness K_T was too large, and this made it difficult or impossible to find an optimized model that agreed with the measurements. To avoid this, the linear optimization was stopped as early as possible to minimize the spring stiffness, K_x, while also minimizing the objective function sufficiently. For this particular model, the best results were found after only 31 iterations. This was the smallest K_x value for which the error between each individual mode frequency was less than 1% in magnitude. See Table 2 for the results. As noted previously, the optimization forces $K_x = K_y$ and $R_x = R_y$.

Table 2: Normalized mode frequency error for the first 6 bending modes (Left). Normalized spring stiffness for each degree of freedom in joints (Right).

Mode Type	Experimental Freq. (Hz)	Model Freq. (Hz)	Error (%)	DOF	Stiffness
Bending	1.0000	1.0001	0.00784	K_x	1
Bending	2.7462	2.7392	-0.25261	K_y	1
Bending	5.3266	5.3176	-0.16668	K_z	0.0264
Bending	8.7025	8.6746	-0.32236	R_x	0.4468
Bending	12.8347	12.7502	-0.65987	R_y	0.4468
Bending	17.5646	17.4679	-0.54919	R_z	0.0375

There is also a torsion mode that has a similar frequency as Mode 5, yet it was not captured well by the model, as elaborated in [18], so it was not included in the optimization.

To understand whether these results represent a global optimum, the effect of changes in spring stiffnesses across all degrees of freedom was investigated. This was done by sweeping one stiffness parameter across a large range of values above and below the optimal value, while holding the rest of the stiffness parameters constant at their optimized values. Figure 3 shows the results of this investigation. In this model, only K_x seemed to have a significant effect on the accuracy of the mode frequencies. R_z was also important, but only for a few modes. There is an interesting trend as K_x is increased, where one by one, each mode reaches a minimum error and then the error increases towards a bound as the stiffness continues to increase. This suggests a tradeoff in error between the modes themselves, where, for example, having a perfectly accurate mode 1 frequency will cause higher error in other modes.

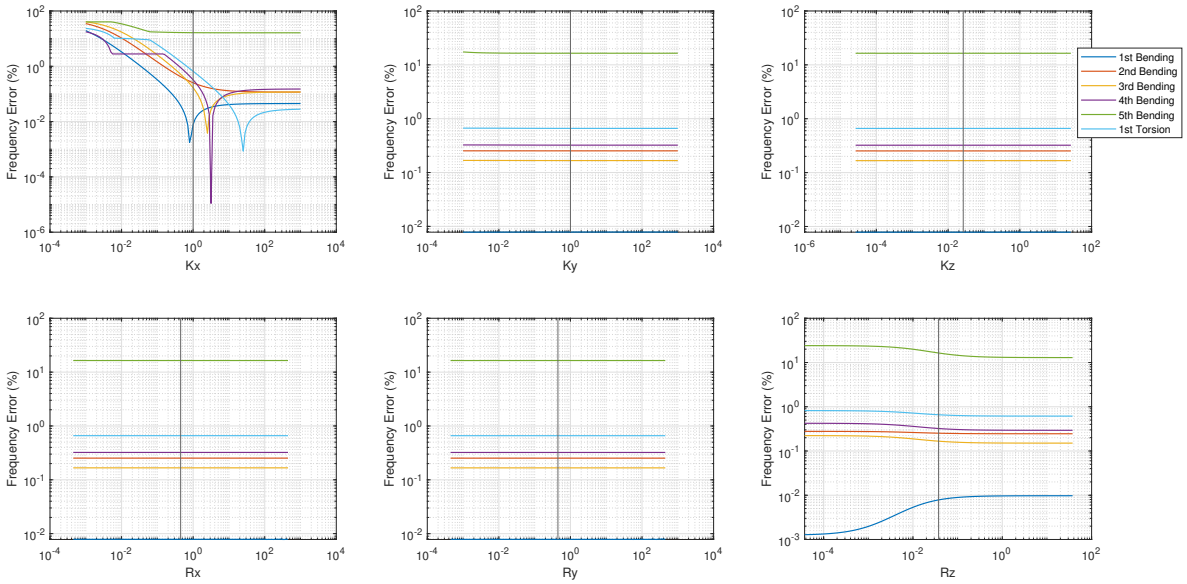

Figure 3: Plots of mode frequency error due to changes in one spring stiffness at a time. Spring stiffnesses are normalized and the vertical lines represent the optimized value for each stiffness parameter.

In our initial attempts at finding the linear spring stiffnesses, it was noted that the modes of the beam would often change order during the course of the optimization. In particular, the first torsion mode of the model is close in frequency to two bending modes, and as the optimization passes through different stiffness values, the torsion mode will change in frequency and switch order with other modes. Figure 4 shows an example of a case in which the mode order changed as the stiffnesses were varied towards their optimal values. Column 6 in Figure 4a is a stiff bending mode and does not match with any experimental mode because measurements were not acquired in that direction. The stiff bending mode moves to column 4 in Figure 4b, which means that the FE modes 4 and 5 have increased in stiffness until they are higher in frequency than the stiff bending mode. The torsion mode is in column 8 of Figure 4a and moves to column 6 of Figure 4b, meaning that its frequency has decreased until it occurs at a smaller frequency than the FE modes 5 and 6. These changes in mode order made it necessary to include a MAC check during every iteration of the linear optimization to ensure that that the correct modes had been matched prior to computing the error in the natural frequencies.

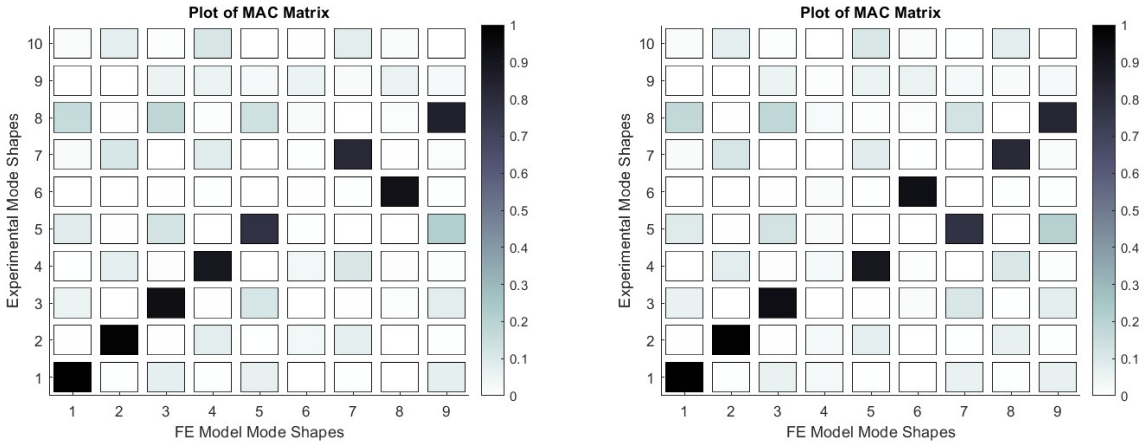

(a) Iteration 15 of optimization.

(b) Iteration 31 of optimization.

Figure 4: MAC plots of linear optimization at two different iterations.

3.3 Nonlinear Iwan Element Model

As explained previously, the four Iwan parameters (K_t, F_s, χ, β) were equal for all 24 Iwan elements and were varied using a Monte Carlo optimization routine, with the goal of maximizing correlation between the measured natural frequency and damping versus amplitude and those of the model. Several insights were obtained while performing this optimization. While it was expected that the most important parameter to the overall performance of the Iwan joint would be the tangential stiffness (K_t), the slipping force parameter (F_s) also affected the performance of the joint by changing the slope of the natural frequency and damping versus amplitude curves of the model. This is illustrated in Figures 5 and 6, where, in Figure 5 the force of slipping is twice the optimized parameter (shown in Figure 6). The increased F_s parameter caused the model to have a smaller slope at high amplitudes in both damping and frequency. The general trend is that a higher F_s causes the QSMA results to have a smaller slope at higher amplitudes and a lower F_s increases the slope of frequency and damping at high amplitudes.

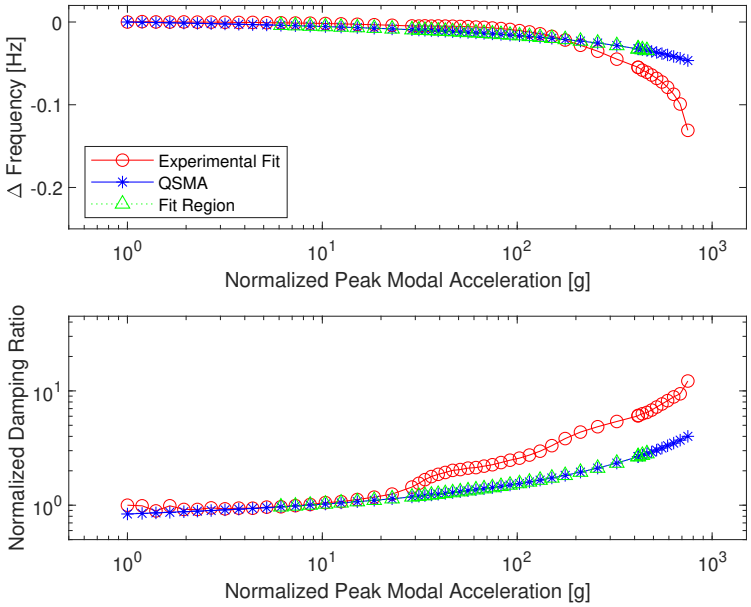

Figure 5: Frequency and damping of Iwan joint model with altered F_s parameter.

As was mentioned previously, while one would ideally leave the K_T value at the stiffness found during the linear optimization, the parameter γ was introduced to allow this to be relaxed. This introduces a tradeoff between the accuracy of the Iwan joint at high amplitudes (i.e. the frequency and damping curves such as those in Fig. 6) and low amplitudes (i.e. the linear mode frequencies). With this in mind, different sets of Iwan parameters were found which prioritize either the accuracy of the

nonlinear frequency and damping ($\gamma < 1$) or the accuracy of the linear frequencies ($\gamma = 1$). These parameters are shown in Table 3.

Table 3: Normalized Iwan parameters with different values of γ. The linear mode frequency errors for Set A are shown in Table 2 while those for Set B are shown in Table 4. The frequency and damping of Mode 1 versus vibration amplitude are shown in Figures 6 and 7 respectively.

Parameter	Set A	Set B
F_s	1.00	0.872
K_t	1.00	0.100
χ	-1.00	-0.727
β	1.00	11.11
γ	1.00	0.10

Using the Iwan parameters in Set A in Table 3, the reduced model maintains the accuracy in terms of linear mode frequency errors shown in Table 2. This model's nonlinear frequency and damping versus amplitude can be seen in Figure 6. This model predicted that the damping would increase by an order of magnitude over the range of magnitudes tested. The model also has reasonable accuracy in matching the changes in frequency however, improvements can be made in matching the curvature of the frequency and damping plots.

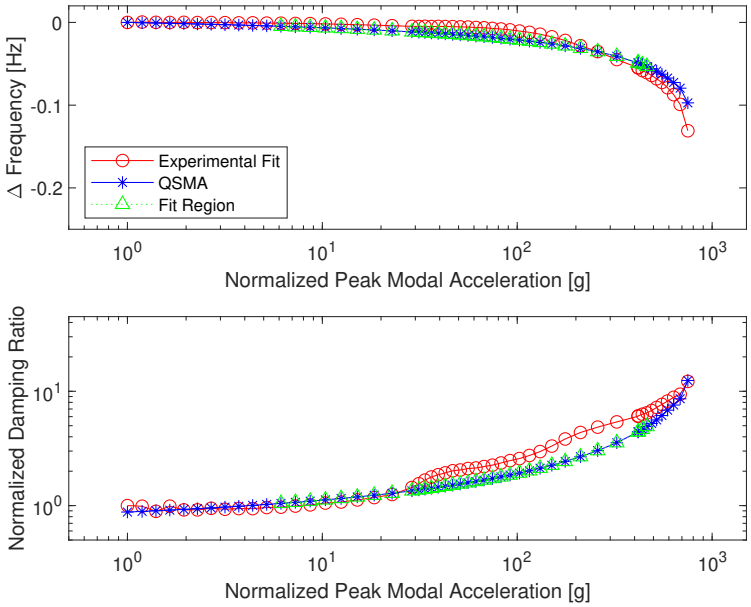

Figure 6: Frequency and damping of Iwan joint model with parameter set A in Table 3 where $\gamma = 1.00$.

As was discussed earlier, tradeoffs can be made to make the nonlinear frequency and damping more accurate, but losing the accuracy of linear mode frequencies. This was explored by changing the parameter γ, which resulted in the Set B Iwan parameters in Table 3. Changing γ changes the K_x stiffness and the linearized natural frequencies of the model. The comparison between model and experimental natural frequencies is shown in Table 4 for the Set B model. As was expected, using γ to scale K_t introduced much more error in mode frequencies, particularly in the higher order modes. The nonlinear response can be seen in Figure 7. With this modified set of Iwan parameters, there is an improved match across the entirety of the tested amplitude range, with exception of the highest amplitudes. The model actually goes into macroslip at the highest amplitudes. The model also slightly overestimates the changes in frequency and damping at the highest amplitudes.

Table 4: Normalized linear mode frequencies of the model with Iwan parameters using $\gamma = 0.10$.

Experimental Freq. (Hz)	Model Freq. (Hz)	Error (%)
1.0000	0.99673	-0.32247
2.7462	2.7067	-1.4371
5.3266	5.1899	-2.5615
8.7025	8.3408	-4.156
12.8347	12.065	-5.9942
17.5646	16.268	-7.3825

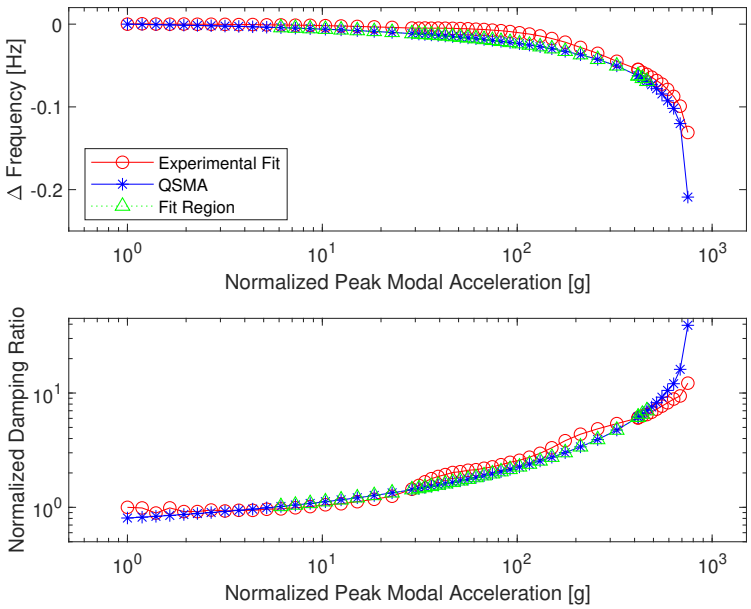

Figure 7: Frequency and damping of Iwan joint model with parameter set B in Table 3 where $\gamma = 0.10$.

Considering both of these alternatives, the authors prefer the model with the Set A parameters with $\gamma = 1$. The Iwan element has the optimal K_x spring constant in that model and hence the linear modes are as accurate as possible. Furthermore, the actual structure is not thought to be on the verge of macroslip at the upper end of the measurement range, so the Set B model with $\gamma = 0.1$ does not seem reasonable. Finally, it should be noted that there is scatter in the experimental measurements, especially with regard to the nonlinear frequency and damping, as elaborated in [17], so it seems unwise to sacrifice agreement in the linear parameters in order to obtain slightly better agreement in the nonlinear response. Furthermore, it is hoped that these two models capture the bounds on the accuracy that is possible with this model and the corresponding experimental hardware and measurements.

4 Conclusions

The approach used in this paper was used in a few prior works [13, 11] on structures with bolted joints. Specifically, similar reduced order models were created and the same optimization approach was used to identify the linear stiffnesses of the joints and the parameters of Iwan elements, which were inserted between the components to capture nonlinearity. This study has shown that this same approach is effective for a structure with many rivets, and good agreement was obtained when the parameters were equal for all rivets.

On the other hand, the study uncovered some important limitations of the optimization approaches that were used. For the structure studied here, as well as that in [11], the stiffness of the Iwan elements needed to be kept low, and in this study manual intervention was required to achieve that. In the future perhaps multi-objective optimization could be used to improve this process. Additionally, the Monte Carlo procedure that was used to find the Iwan parameters was found to struggle when the parameter bounds were large, as they often need to be. This could possibly be addressed by drawing the Monte Carlo samples logarithmically from wide bounds; alternatives should be explored in future works.

This paper considered only the nonlinear behavior of the first mode, but test data is available in [17] for several other modes. The first mode was chosen because it exhibited the strongest nonlinearity, yet the model found here should be checked to see if

it also correctly reproduces the nonlinear behavior of the other modes. This model also has the potential to capture nonlinear modal interactions, and this should also be explored.

References

[1] C Beards. Damping in Structural Joints. *The Shock and Vibration Digest*, 11(9):35–41, 1979.

[2] Matthew R. W. Editor Brake. *The Mechanics of Jointed Structures*. Springer, 2017.

[3] D. J. Segalman, D. L. Gregory, Michael J. Starr, Brian R. Resor, Micheal D. Jew, James P. Lauffer, and Nicoli M. Ames. Handbook on Dynamics of Jointed Structures. Technical report, Sandia National Laboratories, Albuquerque, NM 87185, 2009.

[4] Daniel R. Roettgen and Matthew S. Allen. Nonlinear characterization of a bolted, industrial structure using a modal framework. *Mechanical Systems and Signal Processing*, 84:152–170, 2017.

[5] Mengshi Jin, Matthew R. W. Brake, and Hanwen Song. Comparison of nonlinear system identification methods for free decay measurements with application to jointed structures. *Journal of Sound and Vibration*, 453:268 – 293, 2019.

[6] W. D. Iwan. A Distributed-Element Model for Hysteresis and Its Steady-State Dynamic Response. *Journal of Applied Mechanics*, 33(4):893–900, December 1966.

[7] Daniel J. Segalman. A Four-Parameter Iwan Model for Lap-Type Joints. *Journal of Applied Mechanics*, 72(5):752–760, February 2005.

[8] Hugo Festjens, Gael Chevallier, and Jean-Luc Dion. A numerical quasi-static method for the identification of frictional dissipation in bolted joints. volume 1 of *Proceedings of the ASME Design Engineering Technical Conference*, pages 353–358. American Society of Mechanical Engineers, 2012.

[9] Robert M. Lacayo and Matthew S. Allen. Updating Structural Models Containing Nonlinear Iwan Joints Using Quasi-Static Modal Analysis. *Mechanical Systems and Signal Processing*, 118(1 March 2019):133–157, 2019. Number: 1 March 2019.

[10] A. Singh, M. Scapolan, Y. Saito, M. S. Allen, D. Roettgen, B. Pacini, and R. J. Kuether. Experimental Characterization of a new Benchmark Structure for Prediction of Damping Nonlinearity. Orlando, Florida, 2018.

[11] Aabhas Singh, Wall, Mitchell, Allen, Matthew S., and Kuether, Robert J. Spider Configurations for Models with Discrete Iwan Elements. In *Nonlinear Structures and Systems*, volume 1, pages 25–38, Orlando, Florida, January 2019. Springer.

[12] B. Langrand, L. Patronelli, E. Deletombe, E. Markiewicz, and P. Drazétic. Full scale experimental characterisation for riveted joint design. *Aerospace Science and Technology*, 6(5):333–342, September 2002.

[13] Robert Lacayo, Luca Pesaresi, Johann Gross, Daniel Fochler, Jason Armand, Loic Salles, C. W. Schwingshackl, Matthew S. Allen, and Matthew R. Brake. Nonlinear modelling of structures with bolted joints: a comparison of two approaches based on a time-domain and frequency-domain solver. *Mechanical Systems and Signal Processing*, 114,(1 January 2019):413–438, 2019.

[14] W. C. Hurty. Dynamic analysis of structural systems using component modes. *AIAA Journal*, 3(4):678–685, April 1965. Number: 4.

[15] R. R. Jr. Craig and M. C. C. Bampton. Coupling of Substructures Using Component Mode Synthesis. *AIAA Journal*, 6(7):1313–1319, 1968. Number: 7.

[16] Emily Jewell, Matthew S. Allen, Iman Zare, and Mitchell Wall. Application of Quasi-Static Modal Analysis to a Finite Element Model and Experimental Correlation. *Journal of Sound and Vibration*, 479(4 August):115376, 2020. Number: 4 August.

[17] Suzanna Gilbert, Matthew S. Allen, and Brandon Rapp. Nonlinear System Identification of a Riveted Beam using a Hilbert Transform Based Approach. In *Proceedings of IMAC XLIII*, Orlando, Florida, February 2025.

[18] Cameron Stoker, Josh Blackham, Matthew S. Allen, and Brandon Rapp. Finite Element Modeling for Riveted Joints. In *Proceedings of IMAC XLIII*, Orlando, Florida, February 2025.